Sensors and Materials, Vol. 31, No. 9 (2019) 2997–3006
MYU Tokyo

S & M 1987

Optical and Morphological Studies of Multiwalled Carbon Nanotube-incorporated Poly(3-hexylthiophene-2,5-diyl) Nanocomposites

Nurul Syahirah Nasuha Sa'aya,[1] Siti Zulaikha Ngah Demon,[2] Norli Abdullah,[2] Victor Feizal Knight Ernest Abd Shatar,[3] and Norhana Abdul Halim[2*]

[1]Faculty of Defence Science and Technology, National Defence University of Malaysia, Sungai Besi Camp, 57000 Kuala Lumpur, Malaysia
[2]Centre for Defence Foundation Studies, National Defence University of Malaysia, Sungai Besi Camp, 57000 Kuala Lumpur, Malaysia
[3]Research Centre for Chemical Defence, National Defence University of Malaysia, Sungai Besi Camp, 57000 Kuala Lumpur, Malaysia

(Received July 17, 2019; accepted September 2, 2019)

Keywords: P3HT, carbon nanotubes, optical, vibrational, surface analysis

Conducting polymers are explored as sensing materials owing to their broad interaction with gases and vapours. The sensitivity of a chemiresistive gas sensor can be improved by the incorporation of multifunctional materials such as carbon nanotubes (CNTs). Here, multiwalled carbon nanotube (MWCNT)-incorporated poly(3-hexylthiophene-2,5-diyl) (P3HT) nanocomposite films have been fabricated by solution processing followed by drop casting and spin coating using tetrahydrofuran (THF) as an intermediate solvent. The modification of the absorption peaks observed in UV–Vis spectra was consistent with the observation of the polymer coating onto the MWCNT surface. Fourier transform infrared (FTIR) and Raman vibrational mode spectra of the polymer were obtained after MWCNT incorporation. Coating a polymer onto the nanotube surface was shown to increase the current in the P3HT/MWCNT-OH nanocomposite.

1. Introduction

An enormous number of functional materials have been explored for gas sensing applications owing to the fact that when a particular gas interacts with these surfaces, some alteration in their properties (e.g., optical and electrical properties) can be observed. These functional materials can therefore be considered as sensing films. Because of their flexibility and easy processing, organic and polymer semiconductors have attracted tremendous research attention for use in next-generation electronics and optoelectronics.[1–3] Poly(3-hexylthiophene-2,5-diyl) (P3HT) has been efficiently used as a light absorbing material and employed as a hole-transporting layer owing to its high degree of molecular order via the π–π stacking of adjacent molecules.[3–5] In P3HT-based organic photovoltaic devices, carbon nanotube (CNT)

*Corresponding author: e-mail: norhana@upnm.edu.my
https://doi.org/10.18494/SAM.2019.2513

ISSN 0914-4935 © MYU K.K.

incorporation was found to increase the dissociation rate of excitons as well as the charge carrier collection efficiency.[1,6] CNTs belong to a class of organic materials discovered by Iijima *et al.* in the 1990s that consists of a percolating network of highly conductive CNTs in a polymer matrix.[7,8] Thus, the use of composite nanomaterials such as P3HT/CNT may result in a higher gas-sensing sensitivity.[9] The film processing of conjugated polymers and CNTs has a higher miscibility owing to strong van der Waals interactions between conjugated π-bonds.[10] From self-assembled hierarchical P3HT/CNT supramolecular structures processed by solution crystallisation, P3HT chains grow into nanowires with a stacking direction perpendicular to the CNT axis, increasing the film conductivity.[11]

Previously, many research groups explored P3HT- and CNT-based gas sensors for volatile gas compounds and nerve agent simulants using various sensor architectures.[12,13] In most works, a change in thin film resistivity is used as the main sensing mechanism as $|\Delta R/R_0|$.[12,13] The P3HT/single-walled carbon nanotube (SWCNT) sensor developed by Wang *et al.* has a higher chemiresistive response to dimethyl methylphosphonate (DMMP) than pristine CNT sensors.[9] Several other groups investigated the performance of P3HT chemical sensors that show a fivefold higher sensitivity toward ethanol than acetone.[4,13] P3HT doped with chloroauric acid has been used for selective detection of volatile amines and thiols via colorimetric and chemiresistive methods.[2] The charge carrier density of the doped P3HT thin film is estimated to be ~5×10^{21} cm^{-3}.[2] Selective gas measurement is demonstrated using 30 channel sensor arrays consisting of 15 different polymer/CNT composites to differentiate between several chemical warfare agents and organic solvents.[14] In this paper, we discuss the effect of the regioregularity of different types of multiwalled carbon nanotube (MWCNT) chains on the molecular ordering of P3HT using solution-processed P3HT/MWCNT blend films. The noncovalent functionalization of the CNT and the polymer as the sensing film does not compromise the nanotube backbone; thus, it does not affect the conductivity of the film.[6]

2. Materials and Methods

Regioregular P3HT (molecular weight, M_w ~50000–100000; purity, >99%; Sigma-Aldrich) was used in this work. MWCNTs were purchased from Sigma–Aldrich (purity, >98% carbon basis). Hydroxyl-functionalised MWCNTs (purity, >95%) were purchased from GetNanoMaterials. Tetrahydrofuran (THF) (Sigma-Aldrich) was used as a suspension agent. All materials and reagents were used as received. Nanocomposite films were prepared by the following procedure. MWCNTs were dispersed in THF solution and magnetically stirred at a constant temperature of 50 °C for 96 h. The mixture was then ultrasonicated (f = 50/60 Hz) for 2 h to form a well-dispersed MWCNT suspension. The supernatant of this mixture was collected after centrifuging for 1 h at 4500 rpm. The films were then drop-casted and subsequently spin-coated on α-quartz and indium–tin–oxide (ITO) substrates at 500 rpm for 3 s and allowed to dry at room temperature to volatilise the solvent. Pristine P3HT and P3HT/MWCNT and P3HT/MWCNT-OH nanocomposite films were also prepared with polylactic acid (PLA) as a binding matrix and coated onto thin films for Fourier transform infrared (FTIR)

characterisation. A short spinning duration is used to obtain a uniform thickness and a higher molecular order in the polymer films.[15] A schematic of the procedure for the preparation of the P3HT/MWCNT nanocomposite files is shown in Fig. 1. MWCNTs with different weight ratios of 1:1, 1:2, 1:5, and 1:10 were introduced into the P3HT blend.

Optical characterisation was then performed using a UV–Vis spectrophotometer, an FTIR spectrophotometer, a photoluminescence (PL) spectrophotometer, and a Raman microscope. UV–Vis spectra were recorded using a Genesys TM6 (Thermo Scientific) spectrophotometer at wavelengths of 200−1000 nm. FTIR spectra were recorded on a Perkin Elmer Frontier FTIR spectrophotometer with a resolution of 4 cm^{-1} in the scanning range of 450 to 4000 cm^{-1}. Raman spectra were obtained using a Renishaw Raman microscope with a 50× objective and an excitation beam of 632.8 nm wavelength. PL measurement was performed using a Perkin Elmer LS 55 instrument at room temperature and with an excitation wavelength of 562 nm to obtain information on radiative emissions from photoexcited states of the P3HT/MWCNT composite materials. The microstructure and nanostructure of the samples were studied by optical microscopy, high-resolution transmission electron microscopy (HR-TEM), and field emission scanning electron microscopy (FESEM).

3. Results and Discussion

3.1 Optical studies

The UV–Vis adsorption characterisation provides fundamental information on the material composition, content, and conformation of polymers and the polymer blend when other

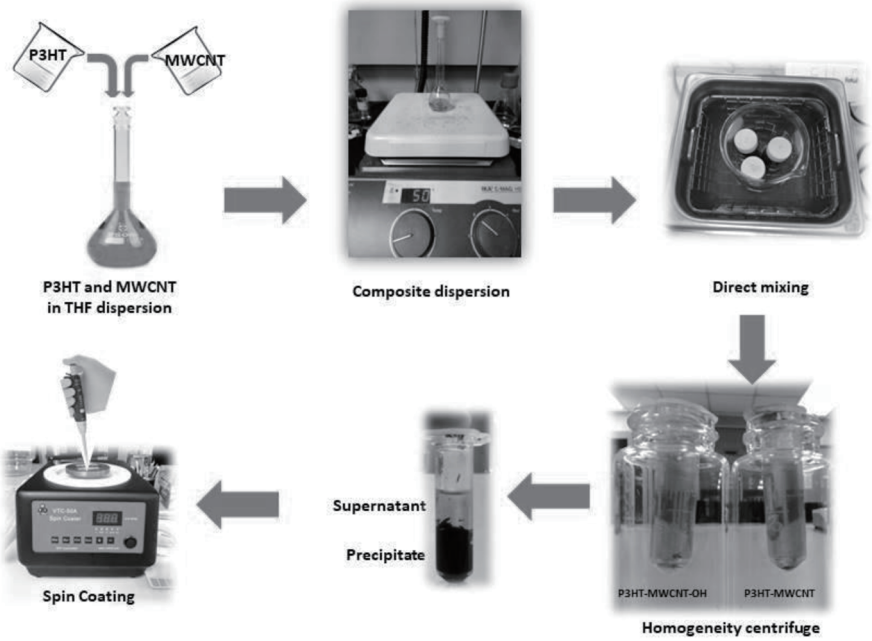

Fig. 1. Schematic procedure for the preparation of P3HT/CNT composite films.

components have been added to a composite.[16] Figure 2 shows the UV–Vis spectra of P3HT/MWCNT dissolved in THF solution at different weight ratios. It was seen that the UV–Vis adsorption spectrum of the P3HT solution is similar to that of P3HT blended with MWCNTs at a ratio of 1:1. This ratio corresponds to the smallest weight of MWCNTs used in our experiment. However, when the weight ratio of the MWCNTs is increased to 1:2, an adsorption peak at a wavelength of 282 nm begins to appear. The adsorption peak at 282 nm related to the CNTs becomes more pronounced as the number of MWCNTs in the blended solution is increased.[17] The calculated optical band gap energies for all blended solutions are shown in Fig. 3. It can be seen that the optical band gap shifts to a higher energy with increasing MWCNT concentration in the polymer solution. The increase in the optical band gap from 2.19 to 2.32 eV is in accordance with Beer–Lambert theory. Beer's law states that the amount of radiation absorbed or transmitted by a solution or medium is an exponential function of the concentration of the absorbing substance present and of the length of the path of the radiation through the sample. A low band gap with good dispersion is desirable for semiconductor materials developed as sensing materials.[18] Therefore, P3HT/MWCNT and P3HT/MWCNT-OH blended films with a weight ratio of 1:1 were selected for further experimental work.

Figure 4(a) shows the UV–Vis spectra of pristine P3HT and P3HT/MWCNT nanocomposite films with a weight ratio of 1:1. In thin-film formations, molecules are stacked against each other and the resulting overlapping π–π bonds give absorption peaks in the visible region. Commercial P3HT strongly absorbs in the region between 450 and 650 nm with two distinct peaks at 562 and 615 nm. These two peaks are attributed to the ordered lamellar phase of P3HT and correlate with the electronic π–π* transition of the aromatic chromophore of the P3HT backbone.[3] The peak at 562 nm can be attributed to the extended conjugated systems, while that at 615 nm is attributed to interchain interactions. It was observed that 562 and 615 nm peaks for pristine P3HT (black) have similar intensities. However, the peak at 615 nm is less prominent for P3HT/MWCNT (grey) and nearly disappears for P3HT/MWCNT-OH

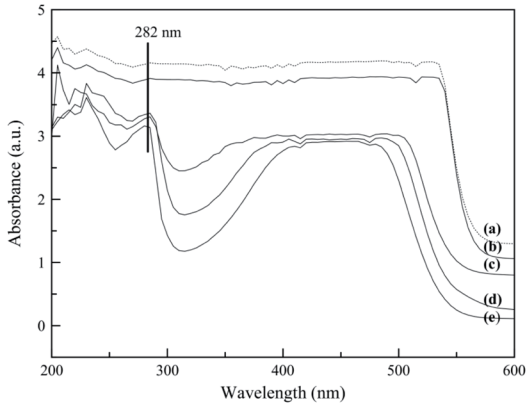

Fig. 2. UV–Vis spectra of (a) pristine P3HT and blended P3HT/MWCNT in THF with weight ratios of (b) 1:1, (c) 1:2, (d) 1:5, and (e) 1:10.

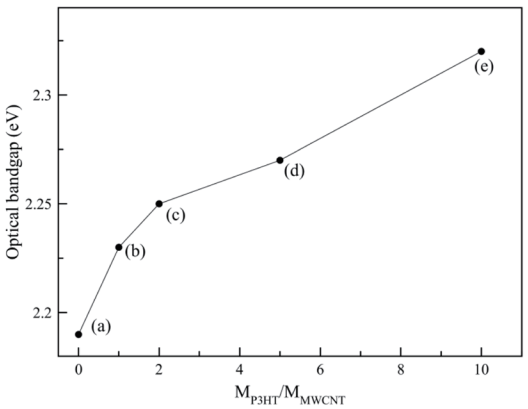

Fig. 3. Optical band gaps of commercial P3HT and P3HT/MWCNT blended solutions with different weight ratios: (a) P3HT pristine, (b) 1:1, (c) 1:2, (d) 1:5, and (e) 1:10 blends.

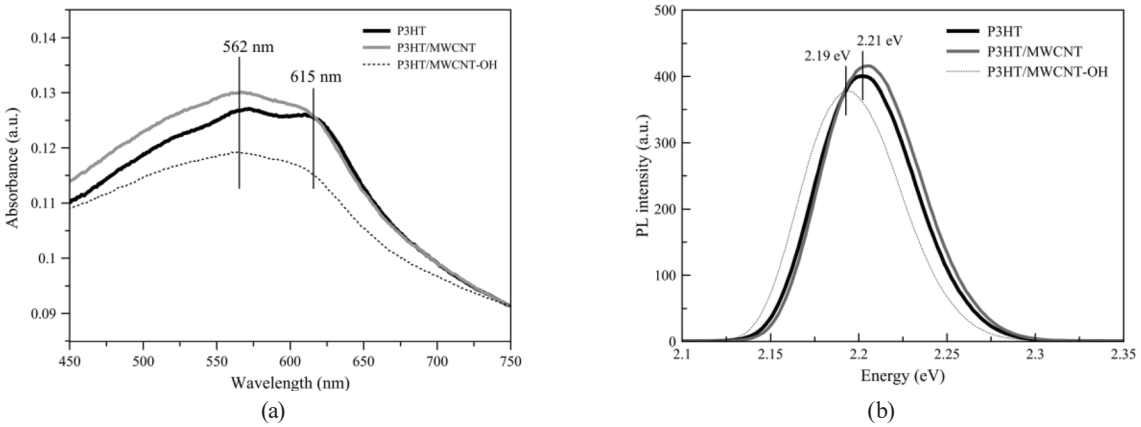

Fig. 4. (a) UV–Vis spectra of pristine P3HT film and P3HT/MWCNT nanocomposite films with weight ratio of 1:1. (b) Normalised PL spectra of pristine P3HT and P3HT/MWCNT and P3HT/MWCNT-OH composite films under 562 nm excitation wavelength.

(dashed). The incorporation of MWCNTs causes the unfolding of the P3HT molecules and their alignment along the nanotubes, resulting in the formation of an ordered structure giving a higher absorption peak at 562 nm than at 615 nm.[5] This same trend was previously observed for P3HT-coated ZnO nanowires.[19]

Figure 4(b) shows the PL spectra of pristine P3HT films and P3HT/MWCNT nanocomposite films under excitation at a wavelength of 562 nm. The PL spectra were obtained to study the radiative emission from photoexcited states of P3HT/MWCNT composite materials corresponding to the π–π* absorption band indicated in the UV–Vis spectra in Fig. 4(a). The P3HT film shows a PL emission peak at 2.21 eV. A small shift was observed for P3HT/MWCNT with a peak at 2.22 eV and the peak of P3HT/MWCNT-OH underwent a redshift to 2.19 eV. The redshift in the PL spectra indicates an increased conjugation length favouring a greater delocalisation of electrons in the polymer chains.[20] In this case, it is shown that MWCNT-OH induces a significant change in polymer conformation owing to the presence of the hydroxyl group.

3.2 Vibrational measurement by FTIR and Raman spectroscopies

Pristine P3HT and P3HT/MWCNT nanocomposite films were further analysed by FTIR spectroscopy, as shown in Fig. 5. An intense peak that originated from PLA appeared at ~1750 cm^{-1} for all films.[21] The P3HT film shows vibrational peaks in three different regions, namely, (i) at 800–1000 cm^{-1} for the thiophene ring, (ii) at 1300–1600 cm^{-1} for the polymer chain, and (iii) at 2800–3100 cm^{-1} for the alkyl chain, which can be attributed to the absorption of a sulfate atom on the thiophene ring, the C=C asymmetric stretching vibration, and the CH_2 out-of-phase stretching of the alkyl chain, respectively.[22] No peak shift was observed in all of the P3HT/MWCNT composite films indicating no strong interaction between P3HT and MWCNTs.[5]

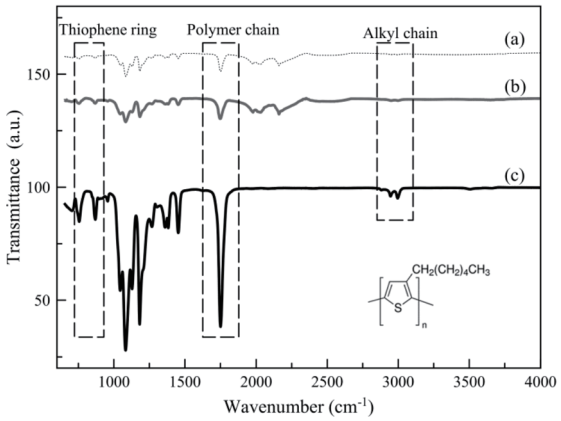

Fig. 5. FTIR spectra of P3HT nanocomposite films (a) P3HT/MWCNT and (b) P3HT/MWCNT-OH, and (c) pristine P3HT.

In another vibrational Raman spectroscopy, only symmetric vibrational mode peaks emerged. Here, peaks that are attributed to the CNTs can be clearly observed. Figure 6 shows Raman spectra of pristine P3HT and the P3HT/MWCNT and P3HT/MWCNT composite films in the range of 1000–3000 cm^{-1}. The peak at 1379 cm^{-1} corresponds to the C–C symmetric bending vibrations of the thiophene ring, whereas that at 1443 cm^{-1} belonged to the symmetric C=C stretching mode of P3HT.[23,24] Both peaks are sensitive to π-electron delocalisation (conjugation length) and thus indicate the degree of molecular order in P3HT films.[23] On the other hand, the intensity ratio of the Raman disorder (D)-band to the graphite (G)-band is often used to estimate the density of structural defects found in CNTs. If both bands are similar in intensity, the density of the structural defects is assumed to be high.[25] A lower band intensity ratio I_D/I_G indicates fewer defects, suggesting a higher structural quality.[5] The peak located at ~1340 cm^{-1} is denoted as the D-band as it is related to scattering from defects and amorphous carbon impurities that are present in the MWCNTs. The second feature with a frequency range from 1550 to 1600 cm^{-1} is referred to as the G-band.[26] The D-band originates from defects and the disordered atomic arrangement of the sp^3-hybridised carbon atoms, whereas the G-band is the result of the G carbon vibrations of the C=C bond.[27] The appearance of the secondary band, the G′-band at 2877 cm^{-1}, is due to the strong coupling between phonons and electrons.[28] It was observed that the intensity of the G-band is higher than that of the D-band for both the P3HT/MWCNT and P3HT/MWCNT-OH films, which highlights the low defect density and the small amount of CNT species.[8] The intensity ratios of the D-band to the G-band (I_D/I_G) for P3HT/MWCNT and P3HT/MWCNT-OH were calculated to be 0.35 and 0.54, respectively. The high defect density of MWCNT-OH is expected for the hydroxyl nanotube functionalisation giving a higher D-band intensity.[7]

3.3 Surface analysis

The microstructures and nanostructures of the films were observed by HR-TEM, FESEM, and optical microscopy. Figure 7 shows the diameter distribution of the as-grown MWCNTs and

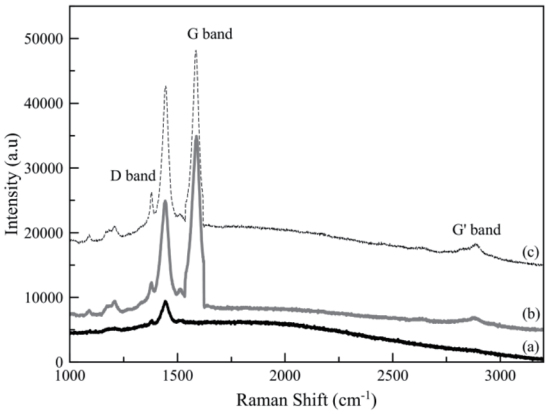

Fig. 6. Raman spectra of (a) pristine P3HT and nanocomposite films (b) P3HT/MWCNT and (c) P3HT/

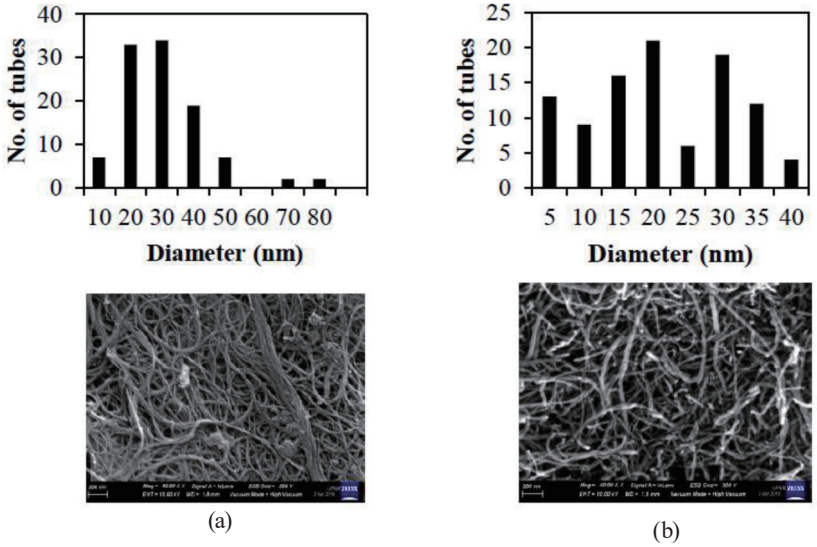

Fig. 7. Population of (a) MWCNTs and (b) MWCNT-OH with different tube diameters determined by FESEM.

MWCNT-OH obtained from FESEM images. The lengths of the MWCNT and MWCNT-OH are 0.5−10 μm and 10−20 μm, respectively. This result shows a narrow dispersion in the diameters found among MWCNT bundles especially for MWCNT-OH. The initial surface analysis of P3HT/MWCNT-OH by laser confocal microscopy shows that the fabricated P3HT may form a nanowire structure as shown in Fig. 8. It is difficult to distinguish the MWCNTs and P3HT in the nanocomposite films; however, the enlarged image in Fig. 8 shows smaller microstructures in a region apart from the aggregated P3HT. These microstructures may be composed of nanofibrillar network structures of P3HT that are responsible for the efficient charge transport pathways in organic devices.[14,29] A previous finding also shows that P3HT can adhere to the CNT surface.[8] The homogeneous dispersion of the CNTs using a polymer as a dispersant will result in the polymer coating on the CNT surface.[30] This geometry of the coating can be confirmed by microscopy techniques.

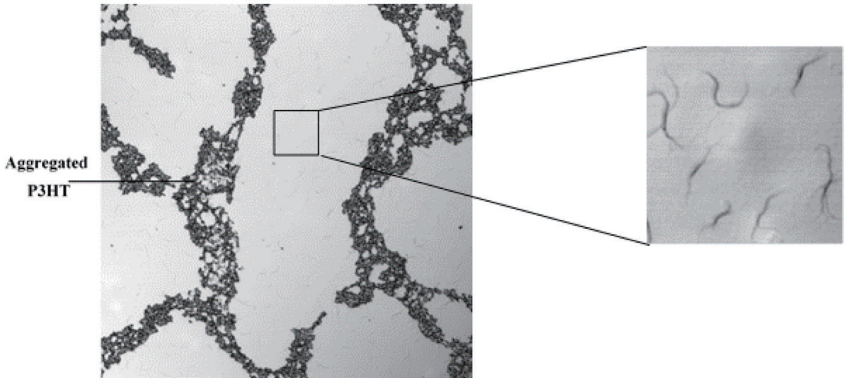

Fig. 8. Photomicrograph of the spin-coated P3HT/MWCNT-OH. nanocomposite film.

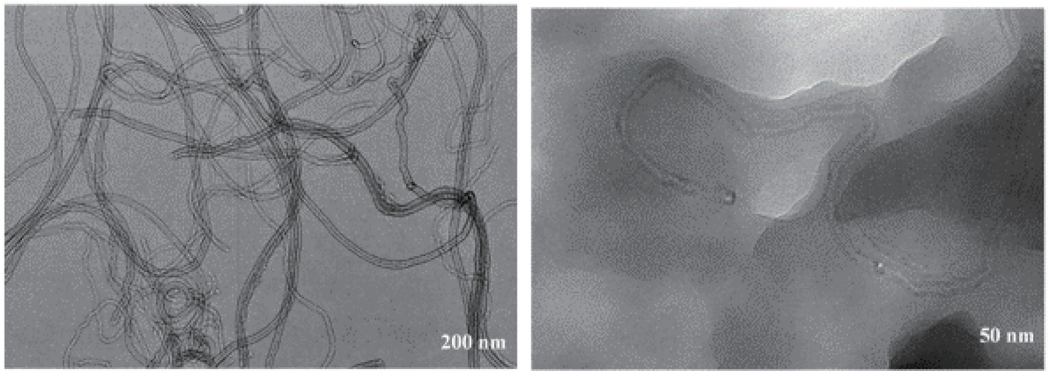

(a) (b)

Fig. 9. HR-TEM images of (a) uncoated MWCNT-OH and (b) P3HT-coated MWCNT-OH.

Figure 9 shows the HR-TEM images of (a) uncoated MWCNT-OH and (b) P3HT-coated MWCNT-OH. Purified MWCNT-OH is seen in an aggregated state [Fig. 9(a)], but after dispersion using P3HT, MWCNT-OH existed in smaller bundles or as individual tubes, as is shown in Fig. 9(b). The polymer-coated MWCNT has ~20 G layers on one side of its wall and polymer bumps can be found attached to the surface of an individual MWCNT-OH. The polymer-coated MWCNT-OH is the reason behind a weaker intermolecular interaction between individual MCWNT-OH tubes, which prevents their aggregation into bundles.[6] This is our successful attempt of coating P3HT onto the surface of MWCNT-OH to be used as the sensing material in the chemiresistor. The P3HT coating on the MWCNT wall can result in a higher degree of π–π stacking on the wall than in the case of bare MWCNT that reflects the modification on the UV–Vis spectra shown in Fig. 4(a). The noncovalent coating of CNTs using various polymers has also been reported by other groups.[6]

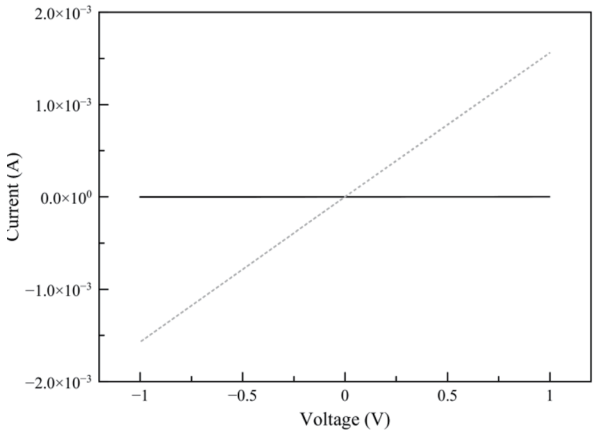

Fig. 10. *I–V* characteristics of P3HT (black line) and P3HT/MWCNT-OH (dashed line) nanocomposite film at scan rate of 100 mV/s.

3.4 Electrical measurement

Figure 10 shows electrical measurements of P3HT and P3HT/MWCNT-OH nanocomposite film obtained using carbon electrodes. Clearly, the effect of MWCNT-OH incorporation facilitated the charge transport property of the P3HT nanocomposite. Mahakul *et al.* have shown a similar marked increase in current up to 8 mA at 20% CNT weightage in the P3HT composite.[5] From the data provided by Sigma-Aldrich, P3HT is a p-type semiconductor with the highest occupied molecular orbital (HOMO) energy level of 5 eV and the lowest unoccupied molecular orbital (LUMO) energy level of 3 eV. Thus, electron migration from the nanotube to the polymer is unlikely to occur owing to the relative position of the Fermi level.[8] However, a new polymer geometry such as P3HT coating/wrapping on the nanotube may consist of the local charge transfer of donor–acceptor interaction that is responsible for the improved conductivity of the device.[5,8]

4. Conclusions

The optical, vibrational, and surface characteristics of P3HT/MWCNT nanocomposites fabricated by a very simple processing method were investigated in our study. One of the key techniques for studying highly sensitive sensing materials is the surface modification of the conducting material. The unfolding of P3HT and decorated/wrapped MWCNTs was observed with a wall thickness up to ~20 G layers. This formation of higher ordered structure on the walls of CNTs is the reason to higher 562 nm absorption peak and reshifted PL peak corresponding to electronic of π–π stacking. An increase in current was observed in the P3HT/MWCNT-OH nanocomposite, indicating the role of decorated MWCNTs in film conductivity.

Acknowledgments

The authors acknowledge the financial support from the Ministry of Education (MoE) and Research Center for Chemical Defence, National Defence University of Malaysia (grant no. UPNM/2018/CHEMDEF/ST/3). Material characterisation was partly carried out at the Malaysia Nuclear Agency and Malaysian Rubber Board.

References

1 T. Hosseini and N. Kouklin: Carbon Nanotubes-Current Progress of Their Polymer Composites (Intech Open Access, 2016) p. 95. https://doi.org/10.5772/62692
2 D. Zhao, L. Li, W. Niu, and S. Chen: Sens. Actuators, B **243** (2017) 380. https://doi.org/10.1016/j.snb.2016.12.018
3 T. Sharma, R. Singhal, R. Vishnoi, G. B. V. S. Lakshmi, S. Chand, D. K. Avasthi, A. Kanjilal, and S. K. Biswas: Vacuum **135** (2017) 73. https://doi.org/10.1016/j.vacuum.2016.10.027
4 P. Powroźnik, A. Stolarczyk, J. Wrotniak, and W. Jakubik, W: Proc. 2017 Eurosensors (MDPI, 2017) 448. https://doi.org/10.3390/proceedings1040448
5 P. C. Mahakul, K. Sa, B. Das, and P. Mahanandia: Mater. Chem. Phys. **199** (2017) 477. https://doi.org/10.1016/j.matchemphys.2017.07.030
6 T. Fujigaya and N. Nakashima: Sci. Technol. Adv. Mater. **16** (2015) 024802. https://doi.org/10.1088/1468-6996/16/2/024802
7 R. Bhatia and L. Kumar: J. Saudi Chem. Soc. **21** (2017) 366. https://doi.org/10.1016/j.jscs.2016.11.003
8 M. Giulianini, E. R. Waclawik, J. M. Bell, M. Scarselli, P. Castrucci, M. Crescenzi, and N. Motta: Polymers **3** (2011) 1433. https://doi.org/10.3390/polym3031433
9 F. Wang, H. Gu, and T. M. Swager: J. Am. Chem. Soc. **130** (2008) 5392. https://doi.org/10.1021/ja710795k
10 S. Charoughchi, S. Agbolaghi, S. Aghapour, R. Sarvari, and F. Abbasi: New J. Chem. **42** (2018) 14469. https://doi.org/10.1039/C8NJ01110A
11 J. Liu, J. Zou, and L. Zhai: Macromol. Rapid Commun. **30** (2009) 1387. https://doi.org/10.1002/marc.200900225
12 K. Manoli, L. M. Dumitru, M. Y. Mulla, M. Magliulo, C. D. Franco, M. V. Santacroce, G. Scamarcio, and L. Torsi: Sensors **14** (2014) 16869. https://doi.org/10.3390/s140916869
13 M. R. Cavallari, J. E. E. Izquierdo, G. S. Braga, E. A. T. Dirani, M. A. Pereira da Silva, E. F. G. Rodrigues, and F. J. Fonseca: Sensors **15** (2015) 9592. https://doi.org/10.3390/s150409592
14 P. K. Chuang, L. C. Wang, and C. T. Kuo: Thin Solid Films **529** (2013) 205. https://doi.org/10.1016/j.tsf.2012.09.024
15 J. Y. Na, B. Kang, D. H. Sin, K. Cho, and Y. D. Park: (2015). Sci. Rep. **5** (2015) 13288. https://doi.org/10.1038/srep13288
16 H. Jin, F. Zheng, W. Xu, W. Yuan, M. Zhu, and X. Hao: J. Phys. D Appl. Phys. **47** (2014) 505502. https://doi.org/10.1088/0022-3727/47/50/505502
17 N. G. Shang, P. Papakonstantinou, S. Sharma, G. Lubarsky, M. Li, D. W. McNeill, A. J. Quinn, W. Zhou, and R. Blackley: Chem. Commun. **48** (2012) 1877. https://doi.org/10.1039/C2CC17185F
18 A. G. Milnes: Solid-State Electronics **29** (1986) 99. https://doi.org/10.1016/0038-1101(86)90029-8
19 A. L. Briseno, T. W. Holcombe, A. I. Boukai, E. C. Garnett, S. W. Shelton, J. J. Fréchet, and P. Yang: Nano. Lett. **10** (2009) 334. https://doi.org/10.1021/nl9036752
20 E. von Hauff: Semiconductors and Semimetals (Elsevier, 2011) p. 231. https://doi.org/10.1016/b978-0-12-391060-8.00007-1
21 S. Z. N. Demon, N. A. Poad, S. H. Jamal, N. F. Rahmat, and N. Bidin: Buletin Optik **2** (2016) 1.
22 P. Larkin: Infrared and Raman Spectroscopy: Principles and Spectral Interpretation (Elsevier, 2011) 1st ed.
23 D. L. Drapcho and T. Hasegawa: https://www.spectroscopyonline.com/applications-infrared-multiple-angle-incidence-resolution-spectrometry?pageID=5 (accessed December 2018).
24 M. V. Ivanova, C. Lamprecht, M. J. Loureiro, J. T. Huzil, and M. Foldvari: Int. J. Nanomed. **7** (2012) 403. https://doi.org/10.2147/IJN.S27442
25 N. A. Mansor, J. P. Tessonnier, A. Rinaldi, S. Reiche, and M. G. Kutty: Sains Malays. **41** (2012) 603.
26 Y. Zhou, Y. Fang, and R. P. Ramasamy: Sensors **19** (2019) 392. https://doi.org/10.3390/s19020392
27 M. S. Dresselhaus and P. C. Eklund: Adv. Phys. **49** (2000) 705. https://doi.org/10.1080/000187300413184
28 S. Kumar, M. Kumar, S. Rathi, A.Yadav, A. Upadhyaya, S. K. Gupta, and A. Singh: AIP Conf. Proc. **1953** (2018) 100074. https://doi.org/10.1063/1.5033010
29 J. S. Kim, J. H. Lee, J. H. Park, C. Shim, M. Sim, and K. Cho: Adv. Func. Mater. **21** (2011) 480. https://doi.org/10.1002/adfm.201000971
30 N. E. Persson, P. H. Chu, M. McBride, M. Grover, and E. Reichmanis: Acc. Chem. Res. **50** (2017) 932. https://doi.org/10.1021/acs.accounts.6b00639